Int. J. Multiphase Flow Vol. 19, No. 5, pp. 803–816, 1993
Printed in Great Britain.

0301-9322/93 $6.00 + 0.00

SEPARATION AND CLASSIFICATION OF AXISYMMETRIC PARTICLES IN AN INCLINED SETTLER

C. ROMERO, J. P. AGARWALA and R. H. DAVIS†
Department of Chemical Engineering, University of Colorado, Boulder, CO 80309-0424, U.S.A.

(Received 23 November 1992; in revised form 2 June 1993)

Abstract—The behavior of axisymmetric particles settling through a quiescent fluid in an inclined settler is studied. The particles undergo Jeffery orbits as they settle, causing their settling rate to vary continually. The orbit-averaged settling velocity is evaluated for any given particle in suspension, and the overall behavior is described by integrating over the probability density function for all particles. Expressions for the degree of classification in an inclined settler (i.e. the particle volume fraction and distribution in the overflow relative to the feed) as the volumetric overflow rate varies are given for: (i) the general case in terms of the distribution of particle size, aspect ratio and orbit constant; (ii) a monodisperse suspension; and (iii) a suspension of equal-diameter cylinders with a log-normal length distribution. Experiments were performed with two monodispersed suspensions of cylinders, and classification results are compared with theoretical predictions. The agreement is within the experimental error, except slightly more particles reached the settler overflow than predicted for the low aspect ratio suspension.

Key Words: sedimentation, Jeffery orbits, axisymmetric particles, inclined settlers

1. INTRODUCTION

Extensive research has been conducted on separating and classifying spherical particles undergoing gravity-induced settling in an inclined settler (e.g. Hill *et al.* 1977; Acrivos & Herbolzheimer 1979; Leung & Probstein 1983; Davis *et al.* 1989), with much of the early work reviewed by Davis & Acrivos (1985). It is found, both from theory and experimental observation, that the sedimentation rate can be greatly increased in an inclined settler over that in a vertical vessel of similar dimensions. This same trend would be expected for nonspherical particles. Synthetic and naturally-occurring particles often deviate significantly from spherical particles, with examples including juice and paper fibers, clays, aggregates, iron filings, red blood cells and many microorganisms. However, the settling behavior for nonspherical particles in inclined vessels has not been quantified previously due to the complexity of the settling behavior of these particles. In particular, the flow fields present in an inclined settling channel cause the suspended particles to rotate or tumble as they settle, and so the sedimentation velocity of an individual particle varies with time.

In a recent publication, Davis (1991) analyzed the settling behavior of axisymmetric particles in a simple shear flow. The particles were assumed to undergo Jeffery orbits (Jeffery 1922) as they settled. A variety of initial orientations was postulated in order to fix the orbit distributions. Davis found that the orbit-averaged particle settling velocities depend only weakly on the initial orientation assumed. In this paper, Davis' work has been extended to predict the settling behavior of suspensions made up of axisymmetric particles in a continuous-flow inclined settler. In particular, the rate of production of clarified fluid in the overflow is predicted, as are the overflow suspension concentration and particle distribution as functions of the imposed flow rate. These predictions are verified by experiments which were performed with two suspensions of cylindrical particles having different aspect ratios.

2. THEORETICAL BACKGROUND

2.1. Axisymmetric particle settling behavior

We consider here suspensions which are sufficiently dilute that the motion of an individual particle is not distributed by neighboring particles. This requires that $nl^3 \ll 1$, where n is the number

†Author for correspondence.

of particles per unit volume and l is their length, so that the volume sampled by a tumbling particle is well-separated from that of other particles. The analysis is also restricted to particles which are sufficiently small that inertia may be neglected, but not so small that rotary or translational Brownian motion is important. When placed in an otherwise undisturbed, simple shear flow, an axisymmetric particle will tumble in the periodic orbits first described by Jeffery (1922). The period of these orbits is

$$T = \frac{2\pi(r_e + r_e^{-1})}{\dot{\gamma}}, \qquad [1]$$

where $\dot{\gamma}$ is the shear rate and r_e is the effective aspect ratio of the particle. For a spheroid, the effective aspect ratio is the same as the true aspect ratio, r, defined as the ratio of the major to minor axis length. For other shapes, a relationship between r_e and r must be determined by computation or experiment. If the particle is nonskew (such as a body of revolution possessing fore-and-aft symmetry), then an imposed body force does not affect the particle's rotation.

The sedimentation velocity of nonspherical particle for creeping flow depends on its instantaneous orientation and is linear in the gravity vector:

$$\frac{\mathbf{U}}{U_S} = \frac{\mathbf{b} \cdot \mathbf{g}}{g}, \qquad [2]$$

where U_S is the Stokes settling velocity of an equal-volume sphere, $\mathbf{g}$ is the gravity vector, $g = |\mathbf{g}|$, and $\mathbf{b}$ is a dimensionless mobility tensor which depends on the particle shape. A single, non-Brownian particle undergoing Jeffery orbits in a shear flow while settling will not deviate from its original orbit unless it is distributed. Its instantaneous velocity will vary continually, but its orbit-averaged velocity will remain constant. Thus, an "orbit-averaged" mobility tensor was described (Davis 1991) by averaging the instantaneous mobility tensor over one full orbit. The theory of Koch & Shaqfeh (1990) suggests that the Jeffery orbits are changed very little by particle–particle interactions in shear flows of semidilute suspension of fibers. Nevertheless, the distribution of orbits will gradually shift away from the initial distributuion due to particle–particle interactions, as observed experimentally by Anczurowski *et al.* (1967). The orbit of any given particle depends not only on the particle shape and size but also on its instantaneous orientation in the shear field. This orientation manifests itself as a constant of integration that arises in the expressions for the orbit-averaged mobility tensor. Due to symmetry, only the diagonal components of the orbit-averaged mobility tensor are nonzero (Davis 1991):

$$\bar{b}_{11} = \frac{b_\perp + r_e b_\parallel}{1 + r_e} - \frac{(b_\parallel - b_\perp) r_e}{r_e(1 + C^2 r_e^2)^{1/2}(1 + C^2)^{1/2} + 1 + C^2 r_e^2}, \qquad [3a]$$

$$\bar{b}_{22} = \frac{r_e b_\perp + b_\parallel}{1 + r_e} - \frac{(b_\parallel - b_\perp)}{r_e(1 + C^2) + (1 + C^2)^{1/2}(1 + C^2 r_e^2)^{1/2}} \qquad [3b]$$

and

$$\bar{b}_{33} = b_\perp + \frac{(b_\parallel - b_\perp)[r_e(1 + C^2)^{1/2} + (1 + C^2 r_e^2)^{1/2}]}{(1 + C^2 r_e^2)^{1/2}[(1 + C^2)^{1/2}(1 + C^2 r_e^2)^{1/2} + r_e(1 + C^2)]}, \qquad [3c]$$

where $b_\parallel$ and $b_\perp$ are the mobilities of the particle parallel and perpendicular to its axis of symmetry, respectively, and are widely available in the literature (e.g. Oberbeck 1876; Batchelor 1970; Gluckman *et al.* 1972) and C is the constant of integration mentioned above, or the orbit constant, and can take on any value from 0 to ∞. An orbit-averaged sedimentation velocity of the particle is then

$$\mathbf{U} = \frac{U_S \bar{\mathbf{b}} \cdot \mathbf{g}}{g} = \frac{U_S(\bar{b}_{11} g_1 \mathbf{e}_1 + \bar{b}_{22} g_2 \mathbf{e}_2 + \bar{b}_{33} g_3 \mathbf{e}_3)}{g}, \qquad [4]$$

where $\mathbf{e}_1$, $\mathbf{e}_2$ and $\mathbf{e}_3$ are the three unit vectors for an orthogonal coordinate system fixed in the laboratory frame of reference. The coordinate system is oriented such that $\mathbf{e}_1$ is in the direction of the imposed shear flow and $\mathbf{e}_2$ is in the direction of its gradient. In general, $\bar{b}_{11} \neq \bar{b}_{22} \neq \bar{b}_{33}$, and so the orbit-averaged sedimentation velocity is not parallel to the gravity vector.

In practice, a suspension will contain an ensemble of sedimenting particles. As long as the suspension is dilute enough so that hydrodynamic interactions between neighboring particles do not significantly disturb their Jeffery orbits or sedimentation velocities, the above development will still hold. In general, the particles will have a distribution of orbits which may be described by a normalized probabilities density function of orbit constant, $P(C)$. Additionally, the particles may not all be identical, resulting in a distribution of values for $b_{\parallel}$, $b_{\perp}$ and r_e.

2.2. The inclined settler

In an inclined settler, particles sediment onto the upward-facing plate of the settler under the influence of gravity. Particles simultaneously settle away from the downward-facing plate of the settler, leaving a thin clear-fluid layer which flows due to buoyancy to the top of the settler. Inclined settlers may be used to clarify fluid, to concentrate a suspension, or to classify particles by taking advantage of variations in settling velocities of the different particles in suspension. Regardless of the intended function of a given inclined settler, one parameter of importance is the clarification rate, $S(\mathbf{U})$, defined as the volumetric rate of production of fluid devoid of particles of settling velocity $\mathbf{U}$. Kinematic considerations dictate that the clarifications rate per unit area must be equal to the scalar product of the particle settling velocity and the vector normal to the surface available for settling:

$$S(\mathbf{U}) = \int_A \mathbf{U} \cdot \mathbf{n} \, dA, \qquad [5]$$

where $\mathbf{U}$ is the sedimentation or relative velocity of the particles to the bulk flow velocity, $\mathbf{n}$ is the unit normal vector pointing outward towards the fluid from the upward facing surfaces of the settler and A is the area available for settling. For dilute suspensions of monodisperse, spherical particles, the vector $\mathbf{U}$ is uniquely described by the Stokes settling velocity of the particles. However, if there are distributions of particle shapes, sizes and/or orbit constants, a distribution of velocities arises. For the current study of particles with axial and fore-and-aft symmetry, the appropriate velocity to use in [5] is the orbit-averaged velocity, $\bar{\mathbf{U}}$, as given by [4], provided that the particle holdup time in the settler is large compared to the period of rotation. The particle holdup time and rotation period depend on the particle properties and on the settler geometry and flow patterns. For low-aspect-ratio vessels, in which the clear-fluid layer is thin compared to the spacing between the inclined walls, the suspension flow is nearly quiescent except near the clear-fluid layer (Acrivos & Herbolzheimer 1979). Thus, particle rotation may not be significant in low-aspect-ratio vessels. On the other hand, high-aspect-ratio vessels, in which the clear-fluid layer thickness is comparable to the spacing between the inclined walls, exhibit strong parabolic flows in both the suspension and clear-fluid layers (Herbolzheimer & Acrivos 1981). Particle rotation will, therefore, be significant in these vessels. Since high-aspect-ratio vessels have both greater clarification rates (per settler volume) and stability (Davis *et al.* 1983), they are the focus of the theory and experiments presented in this paper. Quantitative estimates of the holdup time and rotation period are presented in the section on experiments.

In the present work, we are interested in describing the performance of continuous inclined settlers with a distribution of particle sizes and shapes. Of particular interest is the ability of the settler to separate particles from fluid and also to separate slower-settling particles from faster-settling particles. The settler operation involves pressure-driven flow in which the feed suspension is introduced in the lower portion of the settler, partially clarified fluid containing slower-settling particles is removed through the overflow and concentrated suspension enriched in faster-settling particles is removed through the underflow. For polydisperse or nonspherical particles, there is a distribution of settling velocities and clarification rates. Then, a mass balance on particles of a given settling velocity about the overflow port yields:

$$Q_o X_o P_o(\bar{\mathbf{U}}) = (Q_o - S(\bar{\mathbf{U}})) X_f P_f(\bar{\mathbf{U}}) \quad Q_o > S(\bar{\mathbf{U}}), \qquad [6]$$

where Q_o is the volumetric overflow rate, X_o and X_f are the mass concentrations of particles in the overflow and feed streams, respectively, and P_o and P_f are the corresponding probability density functions. Each probability density function is defined such that $P(\bar{\mathbf{U}})\, d\bar{\mathbf{U}}$ is the fraction of particles by mass having settling velocities in the range $\bar{\mathbf{U}} \pm d\bar{\mathbf{U}}/2$. The above equation is valid, of course,

only if the overflow rate exceeds the clarification rate. Otherwise, the overflow will be devoid of particles of settling rate $\bar{U}$:

$$P_o(\bar{U}) = 0 \quad Q_o \leqslant S(\bar{U}). \tag{7}$$

Equation [6] can be integrated over all particle settling velocities to yield the total concentration of particles in the settler overflow, divided by that in the feed stream:

$$\frac{X_o}{X_f} = Q_o^{-1} \int (Q_o - S(\bar{U}))P_f(\bar{U})H(Q_o - S(\bar{U}))\, d\bar{U}, \tag{8}$$

where $H(Q_o - S(\bar{U}))$ is the Heaviside unit step function, introduced to incorporate the restriction of [7] into the integrated form of [6]. It takes on a value of unity for positive values of the argument, and zero otherwise.

Evaluation of [8] requires that determination of the clarification function, $S(\bar{U})$. Figure 1 is a schematic of a rectangular inclined settler showing the appropriate angles and dimensions. By geometric considerations, the angle between the average sedimentation velocity and the gravity vector is

$$\alpha = \tan^{-1}\left(-\frac{\bar{U}_2}{\bar{U}_1}\right) - \theta, \tag{9}$$

where θ is the angle of inclination of the settler from the vertical. Also, $\bar{U}_3 = 0$ since $g_3 = 0$ for the arrangement shown in figure 1. If the particle length is small compared to the spacing between the inclined walls, h, then the local flow on the particle length scale may be approximated as simple shear, and the particle tumbles in Jeffery orbits. From [4],

$$\frac{\bar{U}_2}{U_1} = \frac{\bar{b}_{22}g_2}{\bar{b}_{11}g_1} = -\frac{\bar{b}_{22}}{\bar{b}_{11}}\tan\theta \tag{10}$$

and so [9] becomes

$$\alpha = \tan^{-1}\left(\frac{\bar{b}_{22}}{\bar{b}_{11}}\tan\theta\right) - \theta. \tag{11}$$

Then, using [5] the clarification rate is the magnitude of the orbit-averaged particle settling velocity multipled by the projected area available for settling:

$$S(\bar{U}) = \bar{U}w[L\sin(\theta + \alpha) + h\cos(\theta + \alpha)], \tag{12}$$

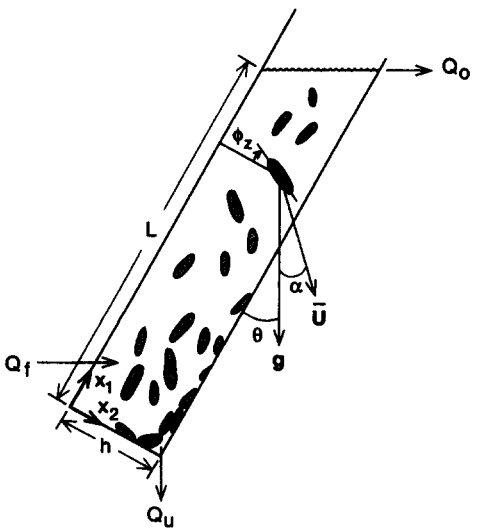

Figure 1. Schematic drawing of an inclined settler. Q_f, Q_u and Q_o are the volumetric flow rates of the feed, underflow and overflow, respectively. The settler is inclined at an angle θ relative to the vertical. A given particle settles with an orbit-averaged velocity $\bar{U}$, at an angle α relative to gravity.

where L, h and w are the length, height and width of the rectangular settler, and $\bar{U} = |\bar{\mathbf{U}}|$. Combining [4] and [12] then yields the desired result:

$$S(\bar{\mathbf{U}}) = U_S w[\bar{b}_{22} L \sin\theta + \bar{b}_{11} h \cos\theta]. \quad [13]$$

Typical vessels are long and narrow ($L \gg h$), and so [13] indicates that the clarification rate increases with increasing angle from the vertical. In general, the desired angle is the largest one which allows the settled particles to still slide down the upward-facing wall of the settler so that they reach the underflow.

Equation [8] may be integrated using [13] for a specified probability density function for the feed suspension, $P_f(\mathbf{U})$. The next section deals with a general form of the integral, the special case of monodisperse axisymmetric particles and the special case of a suspension of cylinders of equal diameters but with a distribution of lengths.

3. THEORETICAL RESULTS

3.1. General suspensions of axisymmetric particles

The orbit-averaged settling velocity of a given particle depends on its size, shape, density and orbit. In general, a suspension of particles will exhibit continuous distributions of sizes, shapes and orbits, whereas the particle densities are more likely to take on only discrete values corresponding to certain materials. Here, we consider only a single particle density, ρ_p. The particle shape is described by its type (cylinder, spheroid etc.) and aspect ratio, r, and the particle oribit is described by its orbit constant, C. The particle size is described by a dimensionless radius, $\xi = a_s/a_0$, where a_s is the radius of a sphere having the same volume as the particle and a_0 is a characteristic radius for the suspension. Then, a dimensionless overflow rate is defined as

$$Q = \frac{Q_o}{U_o w L \sin\theta}, \quad [14]$$

where the Stokes velocity of a sphere with radius a_0 is

$$U_o = \frac{2}{9}\frac{a_0^2(\rho_p - \rho)g}{\mu}, \quad [15]$$

with ρ and μ being the fluid density and viscosity, respectively. The Stokes velocity of an equal-volume sphere for a given particle is then given by

$$U_S = \xi^2 U_o. \quad [16]$$

If the three parameters (r, ξ, C) describing the particle distribution are distributed independently, then [8] may be written as

$$\frac{X_o}{X_f} = \int_0^\infty \int_0^\infty \int_0^\infty \left(1 - \xi^2 \frac{\bar{b}_{22}}{Q}\right) P_f(r) P_f(\xi) P_f(\mathrm{C}) H\left(1 - \xi^2 \frac{\bar{b}_{22}}{Q}\right) \mathrm{d}r\, \mathrm{d}\xi\, \mathrm{dC}. \quad [17]$$

In deriving [17], we have assumed the typical case of high-aspect-ratio vessels ($L \sin\theta \gg h \cos\theta$). Also, $P_f(\mathbf{U})\,\mathrm{d}\mathbf{U} = P_f(r)P_f(\xi)P_f(\mathrm{C})\,\mathrm{d}r\,\mathrm{d}\xi\,\mathrm{d}C$ represents the independent distributions of particle aspect ratio, size and orbit constant in the feed suspension. The probability functions are normalized such that

$$\int_0^\infty \int_0^\infty \int_0^\infty P_f(r)P_f(\xi)P_f(\mathrm{C})\,\mathrm{d}r\,\mathrm{d}\xi\,\mathrm{dC} = 1. \quad [18]$$

For independent distributions, the integral over each parameter is also unity.

3.2. Monodisperse suspensions of axisymmetric particles

A monodisperse suspension ($\xi = 1, r = \text{const}$) of axisymmetric particles settling in an inclined settler will exhibit variations in orbit-averaged sedimentation velocities due only to differences in the orbit constants of the individual particles. Davis (1991) calculated the ensemble-average mobility functions for a variety of orbit distribution functions, $P(\mathrm{C})$. In the present work, we have evaluated the settling behavior for two of these distribution functions. The first corresponds to the

case in which the particles are randomly oriented prior to the onset of shear (i.e. upon introduction to the settler) and follow orbits based on this initial orientation. This neglects the effect of any drift due to Brownian motion or particle–particle interactions, and is given by the Eisenschitz distribution (Eisenschitz 1932). Secondly, we consider the singular distribution proposed by Jeffery (1922), in which all the particles are aligned such that viscous dissipation is minimized. Experimental observations (Mason *et al.* 1956) have shown that in fact particles in a dilute suspension will tend to exhibit a distribution between the Eisenschitz distribution and the singular distribution, after a long time, presumably as a result of occasional particle–particle interactions modifying the oribt constants. Fortunately, the required ensemble-average mobility $\langle \bar{b}_{22} \rangle$, depends only weakly on the chosen orbit distribution for spheroids and cylinders of all aspect ratios (Davis 1991).

For monodisperse suspensions, [17] reduces to

$$\frac{X_o}{X_f} = \int_0^\infty \left(\frac{1-\bar{b}_{22}}{Q}\right) P_f(C) H\left(\frac{1-\bar{b}_{22}}{Q}\right) dC. \qquad [19]$$

The Eisenschitz orbit distribution function is given by (Davis 1991):

$$P_f(C) = mE(k), \qquad [20]$$

where $E(k)$ is the complete elliptic integral of the second kind (Abramowitz & Stegun 1965) and

$$m = \frac{2Cr_e}{\pi(1+C^2)(1+C^2r_e^2)^{1/2}}; \quad k^2 = \frac{C^2(r_e^2-1)}{1+C^2r_e^2}, \quad r_e \geqslant 1 \qquad [21a]$$

and

$$m = \frac{2Cr_e}{\pi(1+C^2r_e^2)(1+C^2)^{1/2}}; \quad k^2 = \frac{C^2(1-r_e^2)}{1+C^2}, \quad r_e \leqslant 1 \qquad [21b]$$

Figures 2 and 3 illustrate the effect of the dimensionless volumetric overflow rate on the relative particle volume fraction in the overflow for various aspect ratios for prolate and oblate spheriods, and for cylindrical rods and discs, using the Eisenschitz distribution. The solid lines represent spheroids, the dashed are cylinders. At low overflow rates, only particle-free fluid enters the overflow and $X_o/X_f = 0$. As the overflow rate increases, particles begin to enter the overflow until, at very high rates, the overflow concentration approaches the feed concentration. For suspensions of elongated particles ($r > 1$, figure 2) or flattened particles ($R < 1$, figure 3), some particles begin to appear in the overflow at much lower overflow rates than for suspensions of particles with aspect ratios close to unity. This is expected due to the higher resistance or lower mobility of the elongated particles. The difference in behavior between cylinders and spheroids of equal geometric aspect ratios is only slight.

Figures 4 and 5 illustrate the sensitivity of the assumed distribution of orbit constants on the volume fraction vs overflow rate profiles for prolate and oblate spheroids, respectively. The solid

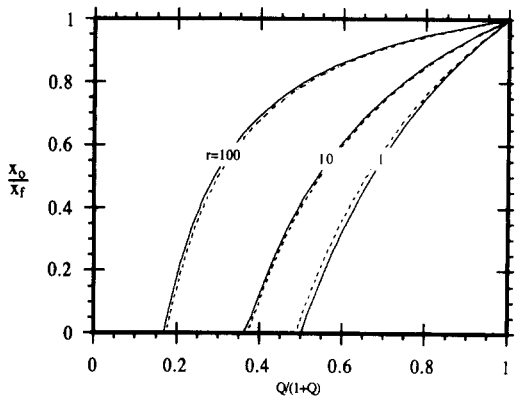

Figure 2. Relative particle volume fraction in the overflow as a function of the scaled dimensionless overflow rate for monodisperse suspensions of prolate spheroids (——) and cylinders (– – – –), with different geometric aspect ratios.

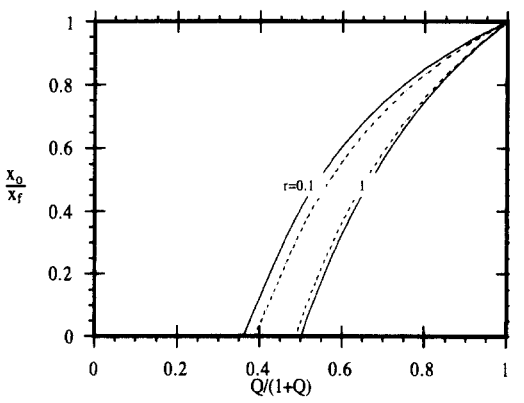

Figure 3. Relative particle volume fraction in the overflow as a function of the scaled dimensionless overflow rate for monodisperse suspensions of oblate spheroids (——) and discs (– – – –), with different geometric aspect.

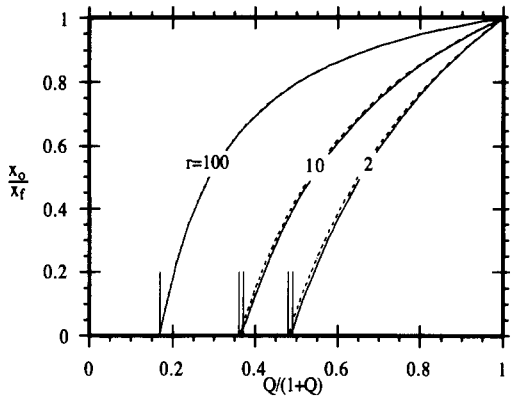

Figure 4. Relative particle volume fraction in the overflow as a function of the scaled dimensionless overflow rate for monodisperse suspensions of prolate spheroids, with an Eisenschitz distribution of orbit constants (——) and a singular distribution with particles aligned with their thin sides in the flow direction (– – – –). Also shown are the overflow rates corresponding to the appearance of the slowest-settling and fastest-settling particles in the suspension (vertical lines).

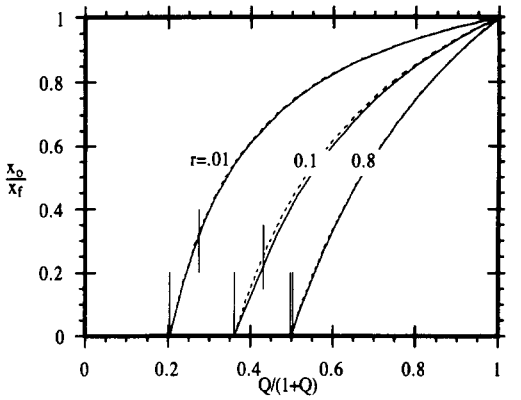

Figure 5. Relative particle volume fraction in the overflow as a function of the scaled dimensionless overflow rate for monodisperse suspensions of oblate spheroids, with an Eisenschitz distribution of orbit constants (——) and a singular distribution with particles algined with their thin sides in the flow direction (– – – –). Also shown are the overflow rates corresponding to the appearance of the slowest-settling and fastest-settling particles in the suspension (vertical lines).

lines represent the Eisenschitz distribution and the dashed lines represent a singular distribution of all particles aligned to minimize viscous dissipation, as first proposed by Jeffery (1992). The effects of the assumed orbit constant distribution do not strongly influence particle sedimentation. This is not surprising since the settler performance depends only on the mobility perpendicular to the flow direction in the plane of shear, $\overline{b}_{22}$, as can be seen from [17]. The Eisenschitz distribution for prolate spheroids and cylinders is skewed towards smaller orbit constants. Even particles of large orbit constants tend to spend the greatest portion of their orbits aligned in the flow direction so that $\overline{b}_{22} \to b_\perp$ in any case. The singular distribution predicts the particle aligned with its primary axis out of the plane of shear, spinning steadily about the axis, so that $\overline{b}_{22} = b_\perp$ in any case. The singular distribution predicts the particle aligned with its primary axis out of the plane of shear, spinning steadily about the axis, so that $\overline{b}_{22} = b_\perp$ also.

A similar effect holds for oblate spheroids and discs. The Eisenchitz distribution is now skewed towards larger orbit constants ($C \to \infty$). This corresponds to an unsteady orbit, with most of the orbit period spent with the thin side of the particle out of the plane of shear and aligned with the flow direction. The singular distribution leading to minimum viscous dissipation is also C = ∞. For oblate spheroids, then $\overline{b}_{22} \simeq b_\parallel$ regardless of the assumed orbit constant distribution.

Two particularly significant values of Q occur for any given monodisperse suspension with a distribution of orbit constants. One is the value of Q at which the slowest-settling particles just begin to enter the overflow. This corresponds to the point at which the curves just begin to rise above the horizontal axis in figure 4 and 5 ($X_o/X_f > 0$). Using [3b], this limit is $Q_1 = \overline{b}_{22} = (r_e b_\perp + b_\parallel)/(1 + r_e)$ for $r_e < 1$ (in which case the solvent-settling particles have C$\to\infty$), or $Q_1 = \overline{b}_{22} = b_\perp$ for $r_e > 1$ (in which case the slowest-settling particles have C = 0). The second significant limit is that for which the fastest-settling particles first appear in the overflow. The limit correspond to $Q_2 = \overline{b}_{22} = b_\perp$ for $r_e < 1$ (C = 0) or $Q_2 = \overline{b}_{22} = (r_e b_\perp + b_\parallel)/(1 + r_e)$ for $r_e > 1$ (C$\to\infty$). These limiting values of Q are indicated in figures 4 and 5 as vertical lines for the suspension exhibiting an Eisenschitz distribution of orbit constants. A greater disparity between the two limits exists for oblate spheroids (figure 5) because the particles that have small orbit constant have high settling mobility ($\overline{b}_{22} \to b_\parallel$ for C$\to$0, $r_e < 1$), whereas the bulk of the particles of high orbit constants have lower settling mobility ($\overline{b}_{22} \to b_-$ for C$\to\infty$, $r_e \to 0$). In contrast, prolate spheroids of *all* orbit constants spend most of their orbit periods aligned such that $\overline{b}_{22} \to b_\perp$ as $r \to \infty$.

Since the orbit-averaged sedimentation velocities of particles in a monodisperse suspension vary with the orbit constant, the overflow will exhibit a different orbit distribution, in general, than the feed. In particular, the overflow will be enriched with the slower settling particles, which corresponds to large orbit constants for $\eta_e < 1$, and to small orbit constants for $r_e > 1$. This would

not be important in applications where the particles are the primary product but it may be of interest for suspensions or composites where controlled particle orientation is desired. The distribution in the settler overflow may be obtained by combining [6]–[8]:

$$P_o(\bar{\mathbf{U}}) = \frac{(Q_o - S(\bar{\mathbf{U}}))H(Q_o - S(\bar{\mathbf{U}}))P_f(\bar{\mathbf{U}})}{\int (Q_o - S(\bar{\mathbf{U}}))H(Q_o - S(\bar{\mathbf{U}}))P_f(\bar{\mathbf{U}})\,d\mathbf{U}}, \quad [22]$$

which for a monodisperse suspension in a vessel with a high aspect ratio becomes

$$P_o(C) = \frac{\left(\frac{1-\bar{b}_{22}}{Q}\right)H\left(\frac{1-\bar{b}_{22}}{Q}\right)P_f(C)}{\int_0^\infty \left(\frac{1-\bar{b}_{22}}{Q}\right)H\left(\frac{1-\bar{b}_{22}}{Q}\right)P_f(C)\,dC}. \quad [23]$$

Figure 6 shows an Eisenchitz initial distribution of orbits for prolate spheroids with $r = r_e = 10$, together with the overflow distribution of orbits for this suspension with $Q = 1$. Note that the overflow distribution is slightly shifted toward smaller orbit constants, which corresponds to particles of lower sedimentation mobility, aligned more in the flow direction. A more pronounced effect is seen for oblate spheroids of $r = r_e = 0.1$, as shown in figure 7. Again, the distributions are the $Q = 1$. Here, the orbit constants in the overflow are shifted towards higher values, corresponding to lower sedimentation rates for oblate spheroids. As discussed previously, the effect on the orbit constant on $\bar{b}_{22}$ is more pronounced for oblate spheroids and discs than for prolate spheroids and cylinders.

3.3. *A distribution of cylinders*

We next consider the case of a suspension containing cylindrical rods of equal radius, a_c, but with a log-normal distribution of lengths, l. This distribution was chosen because it arises in fiber suspension when all particles come from the breakup of fixed-diameter threads, and it may approximate suspensions of certain microogranisms of various ages. The development for this distribution is simpler than the general case given by [17] because the particle size (as measured by a_s or ξ) and aspect ratio are not independent. Instead, the radius of an equal-volume sphere is

$$a_s = (\tfrac{3}{2}r)^{1/2}a_c, \quad [24]$$

where the aspect ratio is defined as $r = l/2a_c$. If a_0 (in the definition of ξ, see [15] and [16]) is chosen as the radius of a sphere having the same volume as a cylinder of aspect ratio $r = \bar{r}_f$, then [17] becomes

$$\frac{X_o}{X_f} = \int_{-\infty}^{\infty}\int_0^\infty \left[1 - \left(\frac{r}{\bar{r}_f}\right)^{2/3}\frac{\bar{b}_{22}}{Q}\right]H\left[1 - \left(\frac{r}{r_f}\right)^{2/3}\frac{\bar{b}_{22}}{Q}\right]P_f(\ln r)P_f(C)\,dC\,d\ln r, \quad [25]$$

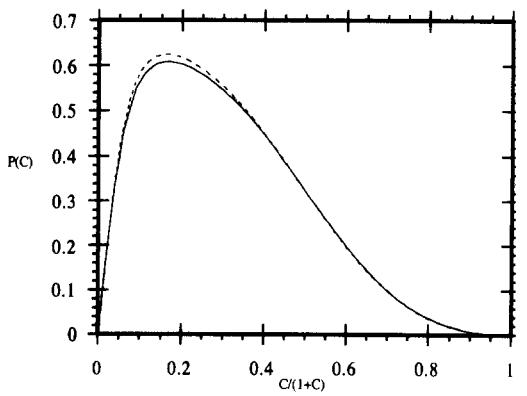

Figure 6. The distribution of orbit constants for monodisperse suspensions of prolate spheroids ($r = 10$) at the dimensionless overflow rate $Q = 1.0$ in the feed (——) and in the overflow (– – – –).

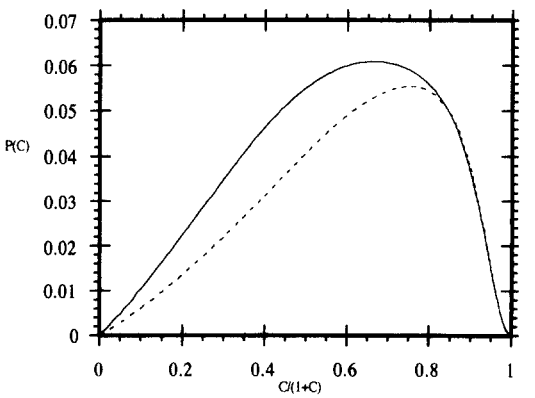

Figure 7. The distribution of orbit constants for monodisperse suspensions of oblate spheroids ($r = 0.1$) at the dimensionless overflow rate $Q = 1.0$ in the feed (——) and in the overflow (– – – –).

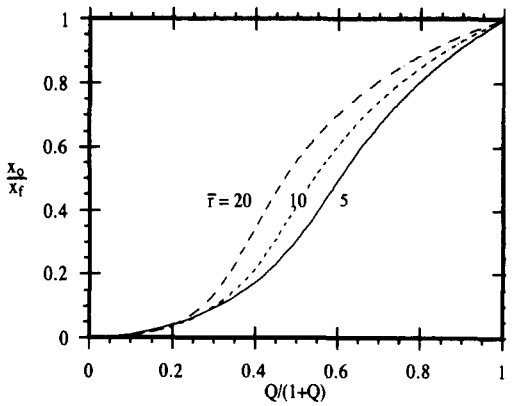

Figure 8. Relative particle volume fraction in the overflow as a function of the scaled dimensionless overflow rate for equal-diameter cylinders with log-normal length distributions having different mean aspect ratios. For all curves, the standard deviation of aspect ratios is $\sigma = 5.0$.

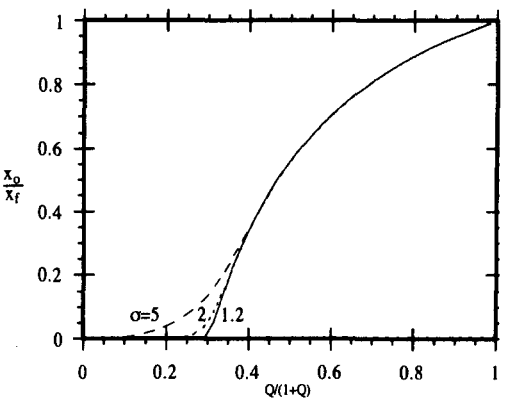

Figure 9. Relative particle volume fraction in the overflow as a function of the scaled dimensionless overflow rate for equal-diameter cylinders having log-normal length distributions. The mean aspect ratio is 20 for all cylinders, and the standard deviation is varied.

where $\bar{r}_f$ is chosen as the mean aspect ratio of the log-normal feed distribution, which is given as

$$P_f(\ln r) = \frac{1}{\sqrt{2\pi}\ln\sigma}\exp\left\{-\frac{1}{2}\left[\frac{\ln\left(\frac{r}{\bar{r}_f}\right)}{\ln\sigma}\right]^2\right\}, \qquad [26]$$

where $\ln\sigma$ is the standard deviation of $\ln r$.

Figures 8 and 9 illustrate the trend of particle content on the overflow with increasing overflow rate for variations in the mean aspect ratio and in the breadth of the distribution, σ. The Eisenschitz distribution is used for $P(C)$. The results are qualitatively similar to those for monodisperse suspensions (figures 4 and 5). However, more of a spread occurs at low overflow rates. This spread is due to the appearance of very short cylinders in the overflow at low overflow rates. In figure 8, the standard deviation is $\sigma = 5.0$ for all curves. In figure 9, the mean aspect ratio is $\bar{r}_f = 20$ for all curves.

Of additional interest is the distribution of aspect ratios for the particles reaching the settler overflow. In particular, the overflow stream will be enriched with the shorter particles and devoid of the longer particles at long overflow rates. For a distribution of cylinder lengths, [22] becomes

$$P_o(\ln r)P_o(C) = \frac{\left[1-\left(\frac{r}{\bar{r}_f}\right)^{2/3}\frac{\bar{b}_{22}}{Q}\right]H\left[1-\left(\frac{r}{\bar{r}_f}\right)^{2/3}\frac{\bar{b}_{22}}{Q}\right]P_f(\ln r)P_f(C)}{\int_{-\infty}^{\infty}\int_0^{\infty}\left[1-\left(\frac{r}{\bar{r}_f}\right)^{2/3}\frac{\bar{b}_{22}}{Q}\right]H\left[1-\left(\frac{r}{\bar{r}_f}\right)^{2/3}\frac{\bar{b}_{22}}{Q}\right]P_f(\ln r)P_f(C)\,dC\,d\ln r}. \qquad [27]$$

This result may be integrated over all orbit constants to yield the distribution of aspect ratios in the overflow stream:

$$P_o(\ln r) = \frac{\int_0^{\infty}\left[1-\left(\frac{r}{\bar{r}_f}\right)^{2/3}\frac{\bar{b}_{22}}{Q}\right]H\left[1-\left(\frac{r}{\bar{r}_f}\right)^{2/3}\frac{\bar{b}_{22}}{Q}\right]P_f(C)\,dC\,P_f\ln r}{\int_{-\infty}^{\infty}\int_0^{\infty}\left[1-\left(\frac{r}{\bar{r}_f}\right)^{2/3}\frac{\bar{b}_{22}}{Q}\right]P_f(\ln r)P_f(C)\,dC\,d\ln r}, \qquad [28]$$

where we note that $P_o(C)$ and $P_o(\ln r)$ are independent distributions which yield unity when integrated over all values of their arrangements, and the mobility $\bar{b}_{22}$ is a function of the aspect ratio r and the orbit cconstant (C). The average aspect ratio of particles in the overflow is then given by

$$\bar{r}_0 = \exp\int_{-\infty}^{\infty}\ln r P_o(\ln r)\,d\ln r. \qquad [29]$$

Figure 10 shows that the predicted size distributions of cylinders in the feed and overflow streams for a log-normal feed distribution with $\bar{r}_f$ and $\sigma = 2$, using an inclined settler with a dimensionless

overflow rate of $Q = 1$. As expected, the overflow distribution is shifted toward the small particles and is completely devoid of particles larger than a critical size ($r = 13.2$) which settle out of suspension before reaching the overflow. The mean particle aspect ratio in the overflow is shown in figure 11 as a function of the dimensionless overflow rate. At low overflow rates, only the shortest cylinders reach the overflow without settling; whereas at large overflow rates, all of the particles reach the overflow and the average size asymptotes to that of the feed distribution. Finally, we note that the underflow is enriched in the larger, faster-settling particles, as may be analyzed using mass balances about the entire settler.

4. EXPERIMENTAL STUDY

4.1. Materials and methods

Cylindrical particles of uniform size were suspended in a viscous fluid and passed through a rectangular settler with $L = 60$ cm, $w = 3.5$ cm and $h = 2.5$ cm. The particles were made by cutting nylon fishing line using a method similar to that described by Bibbo (1987); approximately 50 lines at a time were held tight in a Teflon tube and then cut into prescribed lengths. Two particle sizes were made from two different brands of fishing line, one of aspect ratio $r = 6.25$ ($l = 1250\,\mu$m, $d = 200\,\mu$m) and the other $r = 19.25$ ($l = 3080\,\mu$m, $d = 160\,\mu$m). By finding the composition of a mixture of water and glycerol in which the particles are neutrally buoyant, the densities of the shorter and longer fibers were measured to be $\rho_p = 1.130$ and $1.137\,\text{g/cm}^3$, respectively. The suspending fluid was UCON Heat Transfer Fluid 500, which has density $\rho = 1.034\,\text{g/cm}^3$ and viscosity $\mu = 1.10$ g/cm-s at 25.8°C. The experiments were operated at room temperature without temperature control. The fluid temperature in the vessel was monitored and found to rise 1–2°C over the course of an experiment. However, the temperature at the time when samples were taken and analyzed was always in the range 25.8 ± 0.4°C, with the viscosity varying by $<3\%$ from the reported value and the density varying $<0.1\%$. Under these conditions, the particle Reynolds numbers (based on the diameter and settling velocity of an equivolume sphere) are $<10^{-3}$.

Maximum particle volume fractions of 5×10^{-4} and 5×10^{-5} were maintained during steady-state operation for the particles of aspect ratio 6.25 and 19.2, respectively, corresponding to $nl^3 = 0.025$ and 0.023. The angle of inclination of the settler from vertical was set at $\theta = 15°$ and $\theta = 18°$ for the shorter and longer particles, respectively. For larger angles, it was observed that the settled particles did not readily slide down the upward-facing surface of the channel. A constant overflow rate was controlled by connecting a Masterflex peristaltic tubing pump to the top of the settler. The pump sucked the suspension through the open bottom of the settler from a reservoir, and then returned the overflow stream to the reservoir. The underflow stream was recycled to the

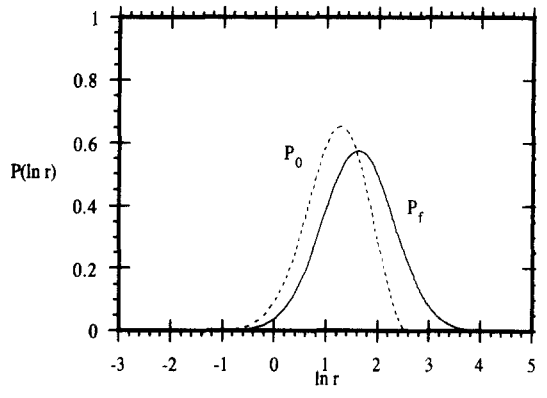

Figure 10. Probability distribution of cylinder aspect ratios in the feed (——) as given by the Eisenschitz distribution and in the overflow (– – – –) for $Q = 1$. The feed is an equal-diameter cylindrical particle suspension have a log-normal length distribution with mean aspect ratio $\bar{r}_f = 5$ and standard deviation $\sigma = 2$.

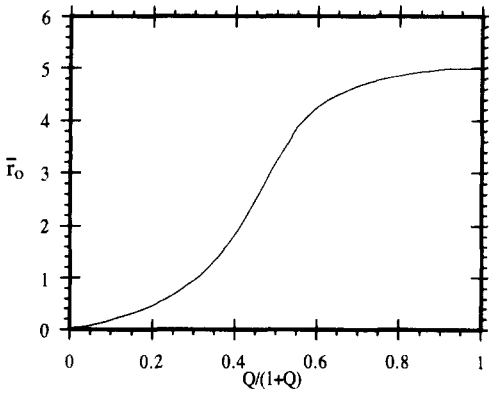

Figure 11. Mean aspect ratio in the overflow as a function of the scaled dimensionless overflow rate for the same particle suspension and conditions as in figure 10.

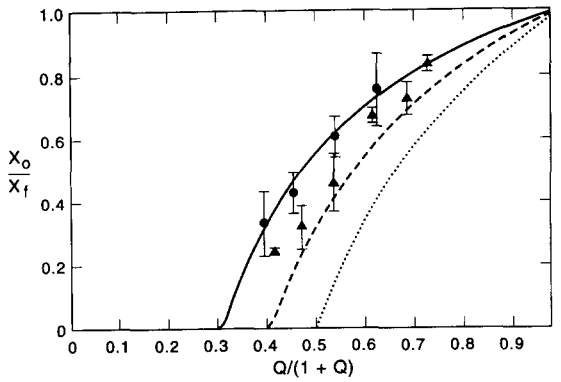

Figure 12. Relative volume fraction of cylindrical particles in the overflow stream for aspect ratios of $r = 6.25$ (△) and $r = 19.25$ (○); the theoretical curves shown are from ([19] and [20] for $r = 6.25$ (– – –), $r = 19.2$ (——) and spheres (· · · · ·).

reservoir by gravity. The overflow rate was varied between 20–80 ml/min. Under these conditions, laminar flow profiles were maintained within the settler. Samples were taken periodically from the reservoir and from the overflow stream. Particle volume fractions in the overflow feed were found by filtering a measured volume of a sample and visually counting the number of particles in the filter. Approximately 2–3 h were required for the concentrations to reach steady state, primarily due to the gradual accumulation of particles on the upward-facing surface of the vessel.

In order to measure the distribution of particle orientations during the flow, a video tape was taken through a magnified lens. This was done for the particles with an aspect ratio of 6.25, since these particles are colored and were clearly visible on the video screen. Approximately 100 particle orientations were measured, and the distribution of particle orientations was found.

4.2. Results and discussion

Figure 12 shows the dimensionless overflow concentration vs the dimensionless overflow rate for both sizes of particles. The data points represent the average of three measurements, and the error bars ± 1 standard deviation. The theoretical curves were calculated using [19] with the Eisenchitz orbit distribution for the feed suspension. Also shown in the plot is the theoretical curve for

Figure 13. Section of a video frame showing cylindrical particle alignment (for $r = 6.25$) in the direction of shear flow; the dark line at the lower left corner of the photo is the lower wall of the inclined vessel and represents the flow direction.

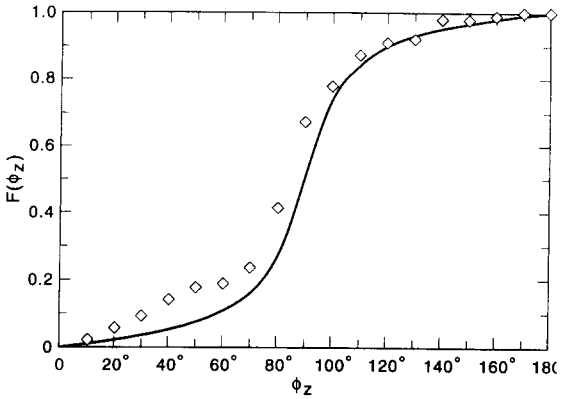

Figure 14. Cumulative distribution of particle orientations for $r = 6.25$; the theoretical curve is from [30], and ϕ_z is defined from 0–180°, with 90° being the direction of flow.

monodisperse spherical particles, which is nearly the same as that for cylindrical particles with an aspect ratio of unity. As the overflow rate is increased, a greater fraction of particles reach the overflow because of the reduction in the suspension holdup time in the settler. For the higher aspect ratio, the theory curve passes through the 90% confidence intervals for all data, whereas half of the data points for the lower aspect ratio are above the theory curve at the 90% confidence level. A variance in particle settling velocities due to interactions may have contributed to this, although the mechanisms giving rise to this variance are not well-understood at present, even for vertical settlers (Koch & Shaqfeh 1989). For a given dimensionless overflow rate, the fraction of particles reaching the overflow increases with increasing aspect ratio; this is because the average settling velocity relative to that of an equal volume sphere decreases with increasing aspect ratio (Davis 1991). The data confirm this prediction, although the difference for the two aspect ratios is statistically significant at only 65% confidence.

A typical video frame for an experiment with the shorter particles is shown in figure 13. The orientation angle ϕ_z between the projection of the particle axis onto the plane of shear (i.e. the plane of the photograph in figure 13) and the velocity gradient (i.e. the direction normal to the inclined walls, or the x_2-axis shown in figure 1) was measured for each particle. The cumulative distribution function, $F(\phi_z)$, defined as the fraction of particles having orientation angles $<\phi_z$, is shown in figure 14. Most of the particles have values of ϕ_z close to 90°, which is consistent with Jeffery-orbit theory in which the particles are predicted to spend more time aligned with the flow than transverse to it. The theoretical curve in figure 14 is the cumulative distribution function given by Anczurowski & Mason (1967):

$$F(\phi_z) = \frac{1}{\pi} \tan^{-1}\left(\frac{\tan \phi_z}{r_e}\right), \qquad [30]$$

where r_e is the effective aspect ratio of the particles. This orientation distribution corresponds to the Eisenschitz distribution in which particles with random initial orientation are assumed to move in undisturbed Jeffery orbits. The effective aspect ratios are $r_e = 5.02$ for $r = 6.25$ and $r_e = 13.2$ for $r = 19.2$ (Davis 1991). For the longer particles, visual observation showed that almost all of the particles were nearly aligned in the direction of flow, as predicted by the theory.

Finally, we note that the theory described in section 2 and 3 is based on the orbit-averaged sedimentation velocity, and so an implicit assumption is that the settler is sufficiently long that the particles undergo several rotations before settling out of suspension. The period of rotation is given by [1]. The characteristic shear rate is the average velocity divided by the channel half-height: $\dot{\gamma} = 2Q_o/(wh^2)$. On the other hand, the holdup time is the settler volume divided by the flowrate: $T_h = whL/Q_o$. An estimate of the number of rotations is then the ratio of the holdup time to the characteristic period of rotation:

$$N = \frac{T_h}{T} = \frac{L}{\pi h(r_e + r_e^{-1})}. \qquad [31]$$

For the particles with $r = 6.25$ ($r_e = 5.02$), $N = 1.5$, whereas for the particles with $r = 19.2$ ($r_e = 13.2$), $N = 0.6$. Thus, the particles did not undergo several rotations, and this was confirmed

by observing the motion of individual particles. However, upon entering the settler, the particles were observed to quickly align with the flow direction and then to rotate slowly until they became unaligned (whereupon they quickly became realigned, consistent with Jeffery-orbit theory). Since the difference between the orbit-averaged settling velocity and that of particles aligned with the flow is only a few percent for particles of the aspect ratios employed (Davis 1991), the insufficient holdup time for several particle rotations is not a significant factor.

5. CONCLUDING REMARKS

The degree of nonsphericity of a particle has a large effect on its settling behavior. In this work, the effects have been quantified for axisymmetric spheriods, cylinders and discs undergoing Jeffery orbits as they settle in an inclined settler. Suspensions of particles that deviate from spherical shapes exhibit the expected behavior of slower setting and, because of this, appear in the overflow at volumetric overflow rates lower than that required for spherical particles to appear. A size classification of nonspherical particles is more difficult than for spherical particles because of varied settling rates of identical particles that are in different orbits. Classification may also be more time-consuming for highly nonspherical particles due to their slower settling velocities. A negligible dependence on the assumed distribution of orbit constants is found for both spheriods and cylinders. Monodisperse suspension of oblate spheroids exhibit a much larger variation in orbit-averaged settling rates than do suspensions of prolate spheroids, due to larger variations in the orbit-averaged sedimentation mobility, $\overline{b}_{22}$, for oblate spheroids with various orbits. For prolate spheroids, $\overline{b}_{22}$ does not deviate far from $b_{\perp}$ over the full range of orbit constants.

Experiments with cylinderical fibers are in reasonable agreement with the theory for the concentration of particles reaching the overflow. Visual observations of the orientation distribution of the cylindrical particles substantiate the use of the Eisenchitz distribution and indicate that most particles align with the flow direction.

Acknowledgement—This work was supported by NSF Grant BCS-8912259.

REFERENCES

ABRAMOWITZ, M. & STEGUN, I. A. 1965 In *Handbook of Mathematical Functions*, p. 592. Dover, New York.

ACRIVOS, A. & HERBOLZHEIMER, E. 1979 Enhanced sedimentation of settling tanks with inclined walls. *J. Fluid Mech.* **92,** 435–457.

ANCZUROWSKI, E. & MASON, S. G. 1967 The kinetics of flowing dispersions: II. Equilibrium orientations of rods and discs (theoretical). *J. Colloid Interface Sci.* **23,** 522–532.

ANCZUROWSKI, E., COX, R. E. & MASON, S. G. 1967 The kinetics of flowing dispersions. IV. Transient orientations of cylinders. *J. Colloid Interface Sci.* **23,** 547–562.

BATCHELOR, G. K. 1970 Slender-body theory for particles of arbitrary cross-section in Stokes flow. *J. Fluid Mech.* **44,** 419–440.

BIBBO, M. A. 1987 Rheology of Semiconcentrated fiber suspensions. Ph.D. Thesis, MIT, Cambridge, MA, pp. 66–69.

DAVIS, R. H. 1991 Sedimentation of axisymmetric particles in shear flows. *Phys. Fluids A* **3,** 2051–2060.

DAVIS, R. H. & ACRIVOS, A. 1985 Sedimentation of noncolloidal particles at low Reynolds numbers. *A. Rev. Fluid Mech.* **17,** 91–118.

DAVIS, R. H., HERBOLZHEIMER, E. & ACRIVOS, A. 1983 Wave formation and growth during sedimentation in narrow tilted channels. *Phys. Fluids* **26,** 2055–2064.

DAVIS, R. H., ZHANG, X. & AGARWALA, J. P. 1989 Particle classification for dilute suspensions using are inclined settler. *Ind. Engng Chem. Res.* **28,** 785–793.

EISENSCHITZ, R. 1932 Die viscosität von suspensionen langgestreckter teilchen und ihre interpretation durch raumbeanspruchung. *Z. Phys. Chem. (Leipzig) A* **158,** 85.

GLUCKMAN, M. J., WEINBAUM, S. & PFEFFER, R. 1972 Axisymmetric slow viscous flow past an arbitrary convex body of revolution. *J. Fluid Mech.* **55,** 677.

HERBOLZHEIMER, E. & ACRIVOS, 1981 Enhanced sedimentation in narrow tilted channels. *J. Fluid Mech.* **108,** 485–499.

HILL, W. D., ROTHFUS, R. R. & LI, K. 1977 Boundary-enhanced sedimentation due to settling convection. *Int. J. Multiphase Flow* **3,** 561–583.

JEFFERY, G. B. 1922 The motion of ellipsoidal particles immersed in a viscous fluid. *Proc. R. Soc. Lond. Ser. A* **102,** 161–179.

KOCH, D. L. & SHAQFEH, E. S. G. 1989 The instability of a dispersion of sedimenting spheroids. *J. Fluid Mech.* **209,** 521–542.

KOCH, D. L. & SHAQFEH, E. S. G. 1990 The average rotation rate of a fiber in the linear flow of a semidilute suspension. *Phys. Fluids A* **2,** 2093–2102.

LEUNG, W. F. & PROBSTEIN, R. F. 1983 Lamella and tube settlers. I. Model and operation. *Ind. Engng Chem. Process Des. Dev.* **22,** 58–67.

MASON, S. G. & MANLEY, R. St. J. 1956 Particle motions in sheared suspensions: orientations and interactions of rigid rods. *Proc. R. Soc. Lond. Ser. A* **238,** 117.

OBERBECK, A. J. 1876 Uber stationäre flüssigkeitsbewegungen mit berücksichtigung der inneren reibung. *J. Reine Angew. Math.* **81,** 62–80.